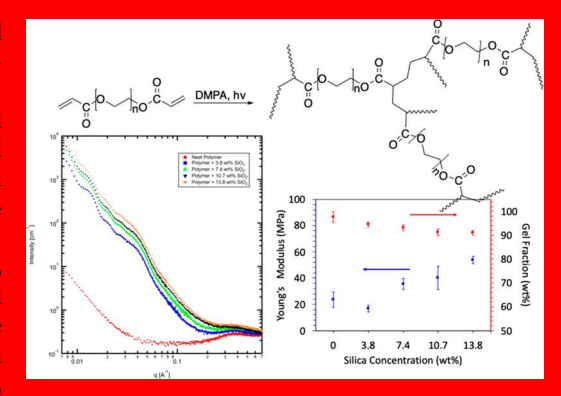


Photocurable Poly(ethylene glycol) Diacrylate Resins with Variable Silica Nanoparticle Loading

Alexis Hocken, Yi Yang, Frederick L. Beyer, Brian F. Morgan, Katelyn Kline, Tyler Piper, and Matthew D. Green*, Too

Supporting Information

Photocurable nanocomposites have tremendous potential in tissue engineering, advanced manufacturing, and structural, multifunctional materials. This project investigates the effect of silica (SiO₂) nanoparticle loading content on the thermal, mechanical, physical, and morphological characteristics of the nanocomposite. An increased concentration of SiO₂ nanoparticles causes a decrease in the gel fraction of the nanocomposite, which, at low nanoparticle loading, degrades the thermal and mechanical properties. However, further addition (>3.8 wt %) causes an increase in the glass-transition temperature, Young's modulus, and ultimate compressive strength. The addition of the nanoparticles had no significant effect on the hydrophilicity according to water uptake experiments. Small-angle X-ray scattering experiments, in conjunction with scanning electron microscopy and transmission electron microscopy, indicated a multimodal particle size distribution and the presence of largescale aggregates.



1. INTRODUCTION

Polymer composites have been studied for decades, because of their ability to join together processable polymer resins with functional additives. 1-8 The additives can range in size from a few nanometers (e.g., 1-5 nm) to several micrometers (e.g., 1-5 μ m) and can be selected for the type of functionality introduced to the matrix, such as electrical conductivity/ insulation, optical characteristics, strength, etc. 9-12 These composite systems boast a density far less than the additive material and are thus touted as lightweight, multifunctional materials. 13 Because of their tunability and the breadth of potential functionalities, they are heavily used within consumer products, construction, nanoelectronics, and biomaterial applications. ^{1,14–17} However, a token disadvantage of polymer nanocomposites is a propensity for nanoparticle agglomeration, caused by depletion forces. There is some evidence that low viscosity and lower-molecular-weight melts afford better nanoparticle dispersions, as indicated by Heinrich and coworkers.18

Polymeric nanocomposites that are cured when exposed to light serve as promising materials for tissue engineering and three-dimensional (3D) architectural applications, because the spatiotemporal cure percentage can be externally controlled.^{1,17,19-21} In addition, photopolymerizations have been explored as alternatives to injection molding, wherein the propagating reactive group moves as a wave through a resinfilled mold; this implementation typically requires a monomer that can undergo cationic polymerization.²² In either case, the composites that are constructed with photoinitiators will form stable, covalently bonded cross-links. In the past decade, a great amount of attention has been devoted to decoupling, or at least understanding the interplay and the polymer chemistry from additive dispersion, as well as to improving composite mechanical properties. 1,3,4,23-28 It has been seen that the incorporation of nanoparticles into the structures can increase the composite's structural integrity. 29,30 Nanoparticles act as anchors to stiffen the polymer matrix, contributing to a morerobust material.31

Recent efforts have sought to further reduce the density of plastic and composite systems by creating porous structures or 3D material designs. The latter must be prepared by additive manufacturing, which restricts the catalog of polymer chemistries available. A photocurable monomer or photoinitiator/monomer system would have to be utilized in order to prepare a 3D thermoset nanocomposite, wherein the resin/ nanoparticle mixture was cured after printing using microstereolithography or technology similar to Carbon 3D (Continuous Liquid Interface Production (CLIP)). 32-35 Thus, photocurable polymer resins, which inherently have a low

Received: April 16, 2019 Revised: July 1, 2019 Accepted: July 18, 2019 Published: July 18, 2019



Department of Chemical Engineering, School for Engineering of Matter, Transport and Energy, Arizona State University, Tempe, Arizona 85287, United States

[‡]U.S. Army Research Laboratory, Aberdeen Proving Ground, Maryland 21005, United States

molecular weight and low viscosity before curing, offer a medium for favorable nanoparticle dispersion 18 that can subsequently be converted to nanocomposites with uniformly distributed nanoparticles. The relative strength of the polymernanoparticle interaction, compared to the nanoparticle-nanoparticle interactions, will play a critical role in achieving uniform dispersions.

To use the nanoparticles to their maximum potential, it is critical to fully understand the fundamentals of their mechanical and physical properties. Specifically, this investigation seeks to understand the influence of SiO₂ loading on the polymerization yield, glass-transition temperature (T_g) , and uniaxial tensile performance. Therefore, we studied a model photocurable polymer nanocomposite system: poly(ethylene glycol) diacrylate monomers loaded with varying weight fractions of 100 nm SiO₂ nanoparticles and a fixed concentration of photoinitiator, which were cured via UV light irradiation. Five different weight loadings of SiO₂ nanoparticles (0, 3.8, 7.4, 10.7, and 13.8 wt %) were tested to elucidate the effects on thermal, mechanical, and physical characteristics of the nanocomposite. The mechanical properties were characterized using compressive testing to determine the Young's modulus, the ultimate compressive stress, and the ultimate strain at break. Physical characteristics, such as the water uptake, the gel fraction, the cross-sectional morphology, and nanoparticle size and size distribution in the composite were determined. Finally, the thermal characteristics were revealed using differential scanning calorimetry (DSC) and thermogravimetric analysis (TGA). This research provides a basis for understanding the mechanical capabilities and chemical properties of hydrophilic, SiO₂-loaded nanocomposite. The ultimate goal is the development of a model system that can be used to make 3D-printable nanocomposites via stereolithography, which will require additional studies at various crosslinker molecular weights, comonomer compositions and ratios, photocatalysts, nanoparticle sizes, and nanoparticle surface compositions.

2. MATERIALS AND METHODS

- 2.1. Chemicals. The poly(ethylene glycol) diacrylate (PEGDA, $M_n = 575$ g/mol, purity of $\geq 99.68\%$) and 2dimethoxy-2-phenylacetophenone (DMPA) were purchased from Sigma-Aldrich. The silicon dioxide (SiO₂) nanoparticles (100 nm in diameter) were purchased from NanoCym. Tetrahydrofuran (THF) was purchased from Fisher Chemical. All materials were used as received.
- 2.2. Composite Fabrication. Composite samples were made by loading SiO2 into PEGDA. To reduce SiO2 aggregation, the nanoparticles were first dispersed in THF (0, 0.04, 0.08, 0.12, or 0.16 g of SiO₂ was added to 3 mL) and sonicated for 40 min. Separately, DMPA was mixed with the PEGDA at a ratio of 0.0035:1 w/w (DMPA:PEGDA). The THF solution was then pipetted into 1.0 g of the DMPA/PEGDA mixture and stirred at 23 °C for 45 min. Next, the THF was evaporated at 23 °C and the solution was transferred into a silicone mold and cured under UV light (wavelength (λ) of \sim 365 nm) for 3 min.
- 2.3. Determination of Sol-Gel Fractions. Soxhlet extraction was used to determine gel fractions. A preweighed sample was placed in the apparatus and >12 complete solvent wash cycles were completed. THF was used as the solvent to dissolve any remaining soluble fraction. The sample was then weighed again after drying under vacuum overnight at 25 °C to determine the final mass (W_f) , which was compared to the initial

mass (W_i) . The gel fraction (C) was calculated according to eq

$$C (\%) = \frac{W_{\rm f}}{W_{\rm i}} \times 100 \tag{1}$$

2.4. Water Uptake Determination. In a standard process, the sample was freeze-dried for 14 h to ensure all water that was absorbed from atmospheric moisture was removed. First, samples were subjected to testing to determine the time required to reach equilibrium. In this equilibrium experiment, the samples were weighed every 30 min until the weight no longer increased (\sim 2.5 h). For each subsequent experiment, all samples were equilibrated for >3 h to ensure maximum water uptake. The sample was then weighed and immersed in deionized water for 3 h to reach the absorption equilibrium.³⁶ The sample was removed from the water and blotted with a cloth to remove excess water on the surface. This sample's mass (W_c) was recorded and compared to its initial mass (W_d) . The percentage (by weight) of water taken up by the network (S) was calculated using eq 2:³⁶

$$S (\%) = \frac{W_{\rm s} - W_{\rm d}}{W_{\rm d}} \times 100 \tag{2}$$

Thermogravimetric analysis (TGA) was performed using a TA Instruments Q500 system. Samples (~5 mg each) were heated at a rate of 10 °C/min from 23-600 °C under nitrogen.

2.5. Characterization of Composites Morphology. The composite cross-sectional morphology was characterized using an environmental scanning electron microscopy (SEM) system (Philips, Model XL30 ESEM-FEG) that was operating at 15 kV. Composite samples were freeze-fractured using liquid nitrogen for cross-sectional examination and sputter-coated with gold before imaging. Small-angle X-ray scattering (SAXS) data were obtained using a camera (Rigaku Americas, Inc., Model S-MAX3000 SAXS) that had a large gas-filled area detector, pinhole collimation optics, and a Confocal Max-Flux collimating optic. X-rays having a wavelength of $\lambda = 1.542$ Å were generated by a rotating copper anode source (Rigaku, Model MicroMax 007HFM). The isotropic two-dimensional SAXS data were corrected for background noise and sample transmission prior to azimuthal averaging into one-dimensional data in the form of intensity (I), as a function of q, where

$$q = \frac{4\pi \sin (\theta)}{\lambda}$$

Here, 2θ is the scattering angle. Distance and beam center calibration were performed using silver behenate. Data were placed on an absolute scale by comparison to a calibrated glassy carbon standard. All data corrections and analysis were performed using Igor Pro v. 7 (WaveMetrics, Inc.) and procedures available from Argonne National Laboratory. 37,38

Transmission electron microscopy (TEM) was performed using a TEM system (JEOL, Model JEM-2100F) that was operated at 200 kV in bright-field mode. Micrographs were collected using an ORIUS SC1000 camera (Gatan, Inc.). Samples of SiO₂ nanoparticles were prepared by drop casting nanoparticle dispersions in either methanol or THF onto carbon-coated TEM grids. The nanoparticle dispersions were made by hand mixing SiO₂ powder in the desired solvent, then dispensed using a micropipette.

2.6. Thermal and Mechanical Analysis. The glasstransition temperature (T_g) was characterized using differential scanning calorimetry (DSC) (Model Q2000, TA Instruments). Samples of 4–6 mg and were sealed into aluminum sample pans. The samples were subjected to a heat-cool-heat process from -100 °C to 200 °C with heating rates of 5 °C/min and a cooling rate of 10 $^{\circ}$ C/min. The midpoint T_g was determined using the T_g function built into TA Instruments' Universal Analysis software. An Instron E3000 device was used to perform compression testing of the SiO₂-loaded nanocomposites. A fresh, dry sample was used for each test. The samples were cut into rectangles and then compressed at a strain rate of 0.1500 mm/min at 23 °C until the sample integrity was compromised.

3. RESULTS AND DISCUSSION

3.1. Synthesis and Characterization. The photoinitiated curing of PEGDA has been well-developed and proposed as a free-radical polymerization mechanism, 20,39 and the synthetic route is shown in Scheme 1. Because the mechanism and kinetics

Scheme 1. Cross-Linking Reaction of PEGDA Initiated by DMPA under UV Light

are understood, as well as the fact that numerous PEGDA chain lengths are commercially available, PEGDA was selected for this investigation. First, the optimal concentration of the photoinitiator was determined by preparing a series of PEGDA hydrogels with various DMPA concentrations without any SiO₂ nanoparticles present (see Figure S1 in the Supporting Information). After curing the resins, the gel fractions were determined using Soxhlet extraction. Briefly, the polymer was washed with an organic solvent in which the monomer is soluble for multiple cycles and the as-cured weight was compared to the weight after rinsing. THF was used as the solvent to dissolve any un-cross-linked monomers or oligomers that remained within the structure. The highest gel fraction was obtained with 0.35 wt % DMPA; therefore, this initiator concentration was used throughout the rest of the investigation.

Next, SiO₂ nanoparticles were added at various weight fractions and the PEGDA oligomers were cured using the same process as described above. Herein, the concentration of SiO₂ nanoparticles is reported as a mass concentration (wt/total wt %), which can be converted to other concentrations (e.g., mol %, vol %), using the reported densities of PEGDA networks and SiO₂ nanoparticles: 1.12 g/cm³ and ~1.9 g/cm³, respectively. 40,41 SiO₂ nanoparticles are common additives in polymer nanocomposites, because of their low cost, tunable hydrophilicity, and the ability to purchase particles across a very broad range of sizes and size distributions. 42,43 The results shown in Figure 1 reveal that the gel fraction decreased as the concentration of SiO₂ nanoparticles increased. This suggests that the SiO₂ nanoparticles inhibit cross-linking by scavenging radicals, limiting diffusion, or simply by diluting the concentration of monomer in the system. Others have observed an acceleration of the polymerization process (involving SiO₂

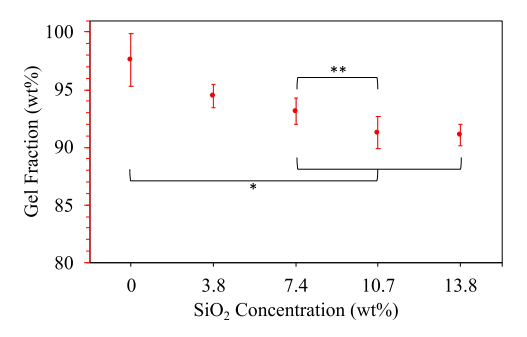


Figure 1. Gel fraction of PEGDA networks with varying SiO2 concentrations. Error bars on the water uptake data indicate the mean \pm one standard deviation. The asterisks indicate statistically significant differences in gel fraction according to the Student's t-test (p < 0.05).

nanoparticles and acrylate-based monomers) but SiO2 agglomeration at higher volume fractions was observed to reduce the reactivity. 44 However, even at the maximum SiO₂ loading of 13.8 wt %, a gel fraction of 91% was achieved. The network with no nanoparticles added exhibited a gel fraction of 100%.

Quantitative measurements of the nanoparticle loading in the hydrogel composites were performed using TGA (Figure 2). The TGA thermograms display dehydration weight losses of \sim 1% at temperatures below 100 °C. This weight loss is due to the desorption of moisture physically adsorbed from the air. A single decomposition step was observed for the series at \sim 360 °C with sharp weight losses of 95.1, 92.4, 85.5, 82.3, and 77.4 wt % as the SiO₂ loading increased from 0 to 13.8 wt %. The weight loss in this step is attributed to the decomposition of the PEG matrix. By correcting for the char weight of the PEGDA matrix, this indicates that the SiO₂ weight percentages of the series were 2.7, 10.1, 12.8, and 17.7 wt % for the 3.8, 7.4, 10.7, and 13.8 wt % SiO₂-loaded nanocomposite samples, respectively. Thus, the TGA data confirm that increasing the SiO₂ nanoparticle loading during synthesis increased the loading in the nanocomposite.

3.2. Characterization of Composite Morphology. The cross-sectional morphology of SiO2-PEG hydrogels was examined using SEM. As shown in Figure 3, the morphology of the series of SiO₂-PEG nanocomposites showed few features at lower nanoparticle loadings (3.8 and 7.4 wt %); however, at higher loadings (10.7 and 13.8 wt %), the nanoparticles became visible. Aggregates containing multiple SiO₂ particles were observed only at 13.8 wt %; however, this does not rule out multiparticle aggregates at lower loadings. At a loading of 13.8 wt %, aggregates of many different sizes were observed with an upper limit of ~500 nm. The bulk morphology and nanoparticle distribution were further probed using SAXS.

The bulk morphological behavior of the nanocomposites was investigated using SAXS, which has been shown to be useful for polymers containing nanoparticle fillers. 45 The resulting data, shown in Figure 4, reveal that the neat polymer is morphologically featureless on the size scale investigated by SAXS (roughly 1 to 100 nm). Addition of the nanoparticles results in a strong increase in scattered intensity at lower angles, with several distinct features in the low-q and mid-q regions. Increasing the SiO₂ content results in a corresponding increase in the scattered intensity. Attempts to fit the above SAXS data using scattering from a monomodal, spherical particle having even a broad size distribution were unsuccessful. Use of a single size distribution allowed a partial fit of the scattering data in the

Industrial & Engineering Chemistry Research

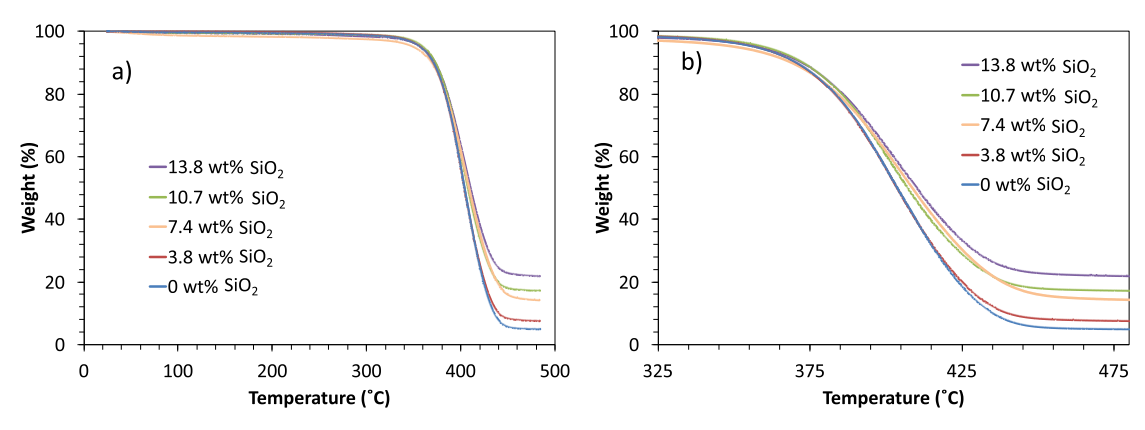


Figure 2. TGA thermograms showing (a) the weight loss from thermal decomposition of the SiO₂-loaded PEGDA nanocomposites and (b) an expanded view of the temperature region where degradation occurs (325–475 °C).

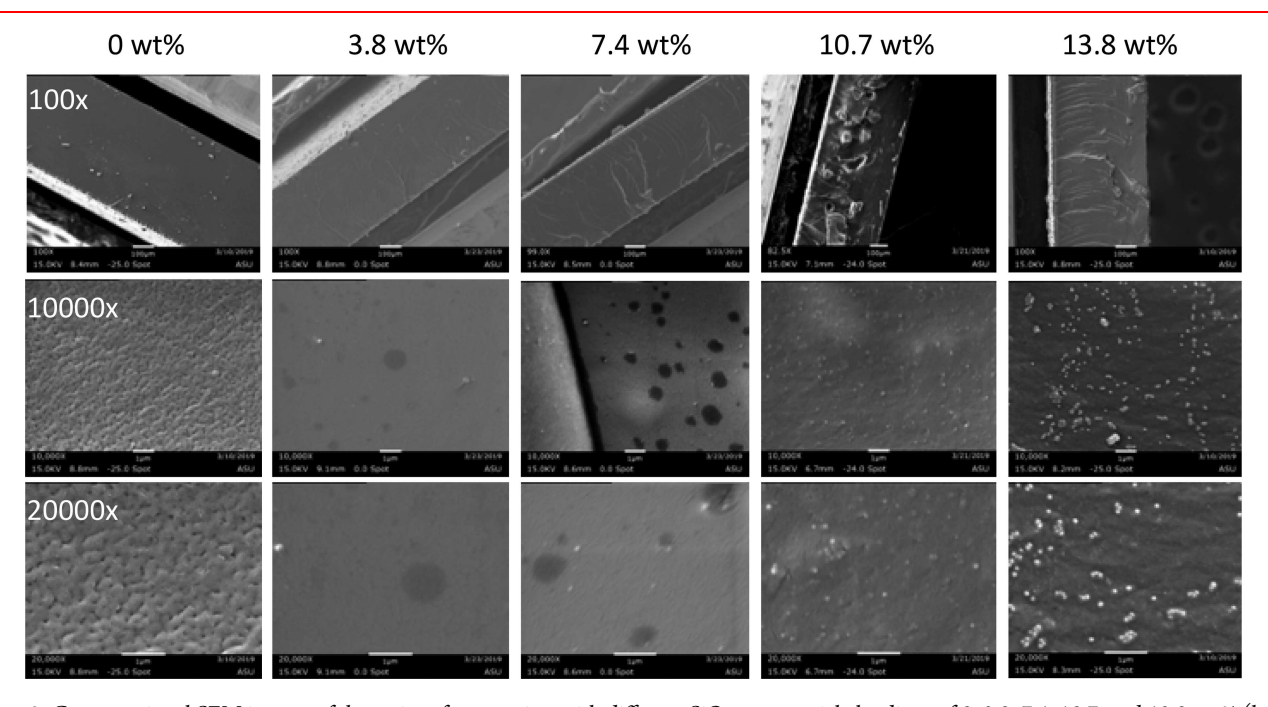


Figure 3. Cross-sectional SEM images of the series of composites with different SiO2 nanoparticle loadings of 0, 3.8, 7.4, 10.7, and 13.8 wt % (left to right), at magnifications of $100 \times$, $10\,000 \times$, and $20\,000 \times$ (top to bottom). The scale bars at $100 \times$, $10\,000 \times$, and $20\,000 \times$ magnifications are $200\,\mu\text{m}$, $20\,000 \times$ μ m, and 1 μ m, respectively.

range of 0.01 Å⁻¹ < q < 0.03 Å⁻¹, but for no other part of the I(q)data. The data were successfully fit using three particle size distributions, having average particle diameters of 82, 12, and 3.2 nm (see the Supporting Information for fitting analysis).

TEM data were collected to provide complementary, real space information on the SiO₂ nanoparticles. Figure 5 (left) shows a representative TEM micrograph of an agglomerate of SiO₂ nanoparticles after dispersion in THF. Several nanoparticles ~85 nm in diameter are visible, along with a large number of nanoparticles ~10 nm in diameter. It appears that nanoparticles having an even smaller diameter are also present. Dispersion of the nanoparticles in methanol revealed this small size component, as shown in Figure 5 (right), having a diameter of ~3 nm. Other researchers have observed that the solvent used for casting nanocomposites can impact the propensity for agglomeration; 46 while these micrographs are of only the nanoparticles, it is important to note that the solvent selected for mixing the nanoparticles with the polymer matrix could impact the nanoparticle size distribution. Given the variation in particle

size observed in TEM and the low-q increase in scattering intensity seen in Figure 4, it is likely that large-scale aggregates exist in these materials.

3.3. Thermal and Mechanical Analysis of the Composites. Water uptake tests were conducted to qualitatively analyze the cross-linking of the composites and determine their relative hydrophilicity. The results, shown in Figure 6 and summarized in Table 1, indicate that the loading of SiO₂ nanoparticles, from 3.8 wt % to 13.8 wt %, does not alter the hydrophilic nature of the cured PEG network in any statistically significant way. The midpoint glass-transition temperatures (T_g) of the SiO₂-PEG nanocomposites were measured as a function of SiO₂ concentration using DSC (Figure 6). Upon the addition of 3.8 wt % SiO₂, the T_{σ} of the nanocomposite decreased by ~2 °C. Further loading of the SiO₂ nanoparticles caused the T_{σ} to increase by 5 °C up to the highest concentration of 13.8 wt %. These reported trends are for the mean T_{o} ; replicate experiments indicate that there is no statistically significant difference in $T_{\rm g}$ at the various SiO₂

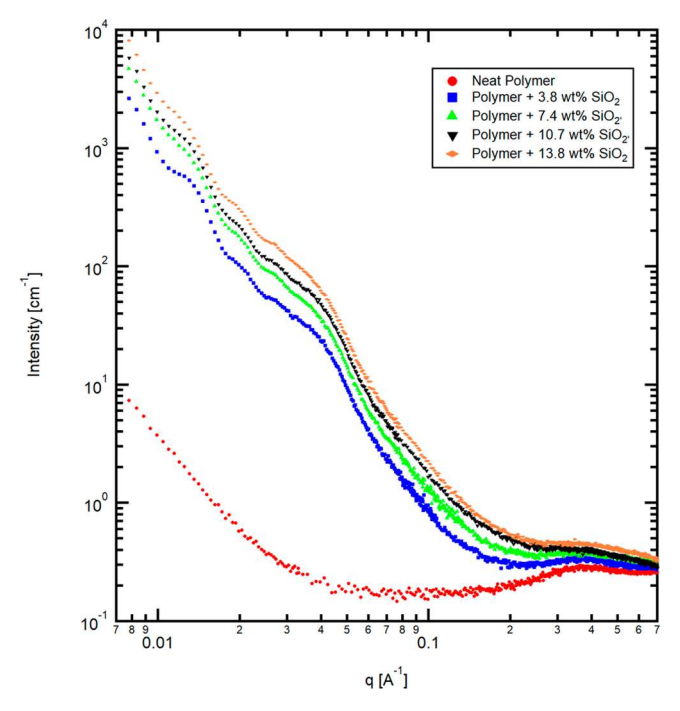


Figure 4. Azimuthally averaged SAXS data from the nanocomposites containing varying amounts of SiO₂ nanoparticles.

concentrations. The initial reduction in $T_{\rm g}$ is attributed to the decrease in gel fraction, which enhanced the segmental mobility by decreasing the restrictions from the network on $T_{\rm g}$. ^{47,48} However, at nanoparticle concentrations of >3.8 wt % the volume fraction and subsequent surface area of interaction between the nanoparticle and the matrix outweigh the decreases observed in gel fraction. ^{48–50} This increased matrix-particle interaction has the effect of restricting segmental motion resulting in an increase in $T_{\rm g}$. We predict that nanocomposites prepared with low weight fractions of nanoparticle that achieved gel fractions of 100% would only display increases in $T_{\rm g}$.

The mechanical properties of the nanocomposites were determined using a static strain rate compression test (Figure 7). The data plotted are representative of three individual runs for each SiO₂ nanoparticle loading. Because of the soft nature of the PEGDA networks, the samples appeared to yield or slip multiple times during the experiment. Upon visual inspection, the sample had not yielded or deformed; these observations were consistent throughout the tensile testing. From the stress—strain curves, the Young's modulus and the ultimate compressive stress were obtained. The Young's modulus was taken as the slope of the stress—strain curve at low strain and was found to be impacted

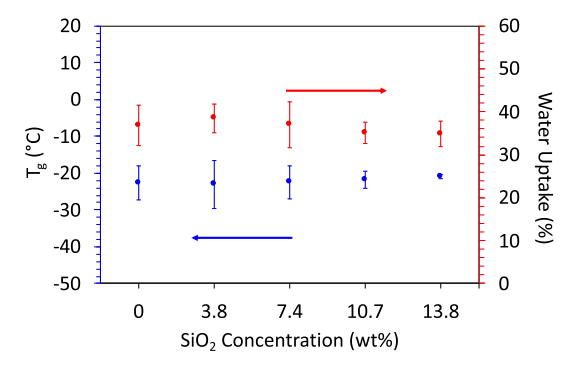


Figure 6. T_g of the composites, as measured by DSC, and the water uptake measured gravimetrically at various SiO_2 nanoparticle concentrations. Error bars on the water uptake data indicate the mean \pm one standard deviation.

by both ${\rm SiO_2}$ concentration and the gel fraction (see Figure 8a). The addition of ${\rm SiO_2}$ had a similar effect on the Young's modulus as it had on $T_{\rm g}$. As previously stated, going from the neat PEGDA network to a ${\rm SiO_2}$ concentration of 3.8 wt % caused a decrease in the Young's modulus, producing a softer network that we attribute to the gel fraction. However, by loading additional ${\rm SiO_2}$ to create a 7.4 wt % composition and beyond caused the reinforcement from the addition of ${\rm SiO_2}$ to outweigh the lower gel fraction. Therefore, the Young's modulus increased as more ${\rm SiO_2}$ is added to the structure at ${\rm SiO_2}$ concentrations of >3.8 wt %. Interestingly, the Young's modulus did not decrease at high loadings, which is a hallmark of nanoparticle aggregation at high volume fractions. This data, together with the cross-sectional SEM, possibly rules out percolation of the spherical nanoparticles, but does not rule out aggregates altogether.

The effect of the multimodal particle size distribution must also be considered in the context of this mechanical performance data. Previous work has demonstrated that particle size and particle size distribution do not impact the Young's modulus and tensile strength of the composite. Some qualification is needed to contrast these findings with our data, including the particle size $(50-350 \, \mu \text{m})$ and the uniform size distributions of the particles. It is possible that the multimodal size distribution herein could impact the composite performance, which will be the subject of future investigations.

In addition to the Young's modulus, the tensile testing showed that the higher SiO_2 nanoparticle concentration (>3.8 wt%) increased the strain at break and had an impact on the ultimate compressive strength (UCS) (see Figure 8b). At low nanoparticle concentrations, the effect of the lower gel fraction was dominant, causing a softer sample with a lower UCS (similar to the trend observed for T_g and Young's modulus). However, after

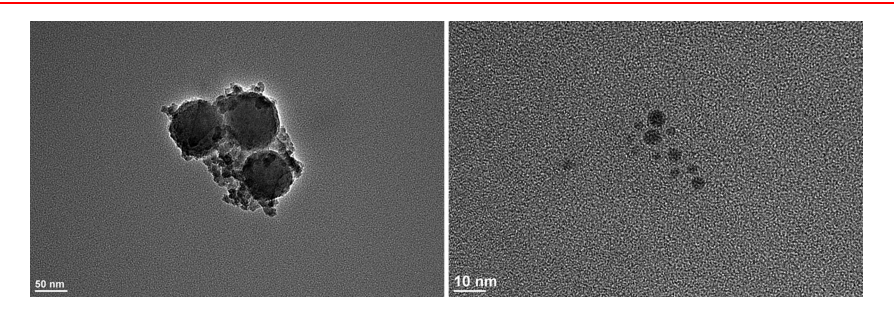


Figure 5. (left) An agglomerate of SiO_2 nanoparticles with various diameters, after drop-casting from THF. (right) An aggregate of SiO_2 nanoparticles with diameters of \sim 3 nm, after drop-casting from methanol.

Table 1. Summary of the Gel Fraction, Water Uptake, Glass-Transition Temperature, Young's Modulus, and Ultimate Compressive Stress of the Series of Nanocomposites with Different SiO₂ Loadings

amount of SiO ₂ nanoparticles (wt %)	gel fraction (%)	water uptake (%)	glass-transition temperature, $T_{\rm g}$ (°C)	Young's modulus (MPa)	ultimate compressive stress (MPa)
0	98 ± 2.3	36.9 ± 4.7	-22.6 ± 4.7	23.58 ± 5.94	3.54 ± 0.87
3.8	95 ± 1.0	38.5 ± 3.3	-23.0 ± 6.5	16.80 ± 2.53	2.52 ± 0.73
7.4	93 ± 1.1	37.0 ± 5.4	-25.6 ± 4.4	35.43 ± 4.34	5.86 ± 1.40
10.7	91 ± 1.4	35.2 ± 2.5	-23.5 ± 2.4	40.10 ± 8.75	8.55 ± 2.90
13.8	91 ± 0.9	34.9 ± 2.9	-20.4 ± 0.6	53.83 ± 2.70	9.22 ± 3.14

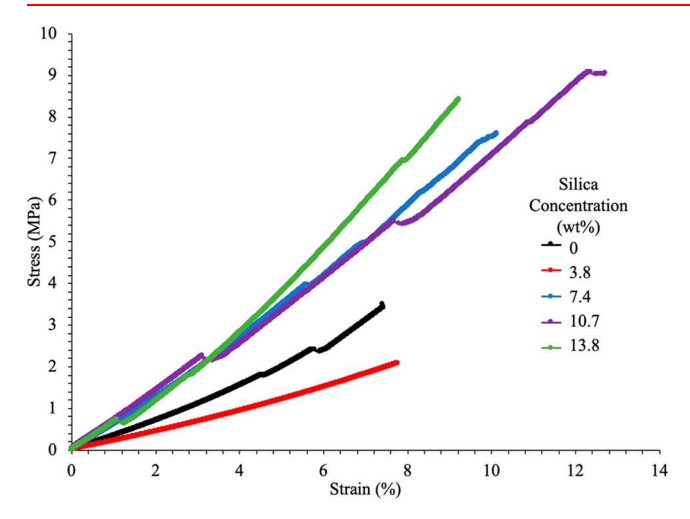


Figure 7. Tensile testing of the SiO_2 -loaded nanocomposites in compression mode at a strain rate of 0.150 mm/min. These traces are representative plots of three individual runs per SiO_2 loading.

adding more nanoparticles to achieve a 7.4 wt % composite, the reinforcement from the nanoparticles overcame the negative effects of the decreasing gel fraction. Thus, the ultimate compressive strength increased as the nanoparticle loading increased. Collectively, these data suggest that the limited segmental mobility (relatively high T_g) contributed by loading SiO_2 nanoparticles at ~10 wt % overcomes the negative effects of an increased gel fraction, and also enhanced the mechanical strength 2-3 times, relative to the unloaded sample.⁵³ Additional testing to determine the effect of the molecular weight between cross-links is needed in order to decouple gel fraction and thermal and mechanical properties. However, the ultimate compressive modulus of SiO₂-loaded nanocomposites falls within the range needed for soft tissue engineering (\sim 0.4– 350 MPa). 54,55 The added benefit of using photocuring techniques affords hierarchical designs through stereolithographic 3D printing or photopatterning. The material system

investigated herein requires additional engineering to enable these advanced processing techniques. Moreover, reducing the molecular weight between cross-links will dramatically increase the composite modulus, opening up alternative applications requiring harder, rigid material properties. The absolute values for the $T_{\rm g}$ gel fraction, water uptake, Young's modulus, and UCS, as a function of SiO₂ concentration, are summarized in Table 1

Collectively, this investigation begins to demonstrate how systems with varying amounts and types of photoinitiators, monomers, and nanoparticles could be utilized to prepare 3D hierarchical composites. However, as noted above, additional studies are needed to decouple the effects of cross-linker molecular weight, comonomer composition and ratio, photocatalyst (e.g., wavelength, half-life, and efficiency), nanoparticle size, and nanoparticle surface composition on the curing kinetics and composite performance. Furthermore, additional investigations into the polymerization process (e.g., heat-release profile 56-59 and radical/ion propagation), amenability to patterning, 60,61 and optical characteristics will be necessary along with comprehensive kinetic studies. Finally, additional strategies to control and characterize nanoparticle dispersion will be crucial before this material system can be implemented in an advanced manufacturing technique such as 3D printing.

4. CONCLUSIONS

 SiO_2 –PEG nanocomposites exhibit qualities that are promising for tissue engineering, advanced manufacturing, and multifunctional materials. Higher concentrations of the SiO_2 nanoparticle limited the gel fraction obtainable and had no impact on the water uptake experiments. At low loadings (<3.8 wt %), the T_g , Young's modulus, and UCS all decreased. However, the addition of SiO_2 nanoparticles at concentrations from 3.8 wt % to 13.8 wt % resulted in a monotonic increase in T_g , Young's modulus, and UCS. Cross-sectional SEM and SAXS experiments indicated that some fraction of the particles existed as 82, 12, or 3.2 nm particles, all of which were also observed in TEM imaging of the nanoparticles. In summary, the low density of the

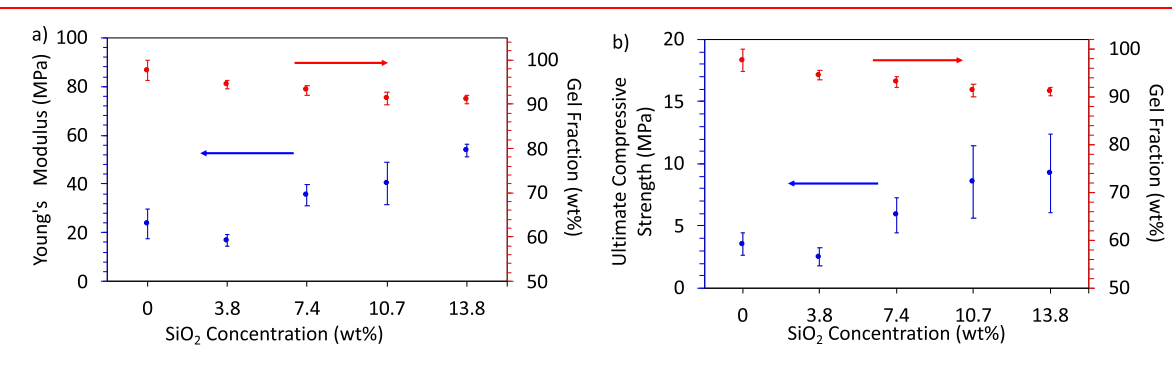


Figure 8. (a) Young's modulus and (b) ultimate compressive strength, as a function of SiO₂ nanoparticle concentration and gel fraction.

SiO₂-loaded nanocomposite gives way to creating a lightweight and multifunctional material. The tunability of this material, combined with its amenability to photoactivated polymerization, suggests that 3D and hierarchical assemblies are nearterm possibilities.

ASSOCIATED CONTENT

Supporting Information

The Supporting Information is available free of charge on the ACS Publications website at DOI: 10.1021/acs.iecr.9b02068.

Synthesis optimization: photoinitiator concentration study, cross-section SEM images, SEM images of SiO₂ nanoparticles, DSC traces, and a SAXS-fit model used to determine the SiO₂ particle sizes (PDF)

AUTHOR INFORMATION

Corresponding Author

*E-mail: mdgreen8@asu.edu.

ORCID ®

Frederick L. Beyer: 0000-0003-0253-2134 Matthew D. Green: 0000-0001-5518-3412

Present Address

 $^{\nabla}$ Now at Olin Corporation, Freeport, TX.

The authors declare no competing financial interest.

Biographies



Alexis Hocken is a third-year Bachelor's student in the honors college at Arizona State University, pursuing a degree in Chemical Engineering with a minor in Biochemistry. She has been conducting research in Professor Matthew D. Green's lab since late spring 2018, where she developed her interest in nanomaterials for biomedical applications. Alexis is a ASU/NASA Space Grant Scholar as well as a DAAD RISE Scholar, where she conducted drug delivery research at the Otto-Schott Institute for Materials Research in Jena, Germany.



Yi Yang is currently a postdoctoral researcher working on direct CO₂ capture in the School for Engineering of Matter, Transport and Energy at Arizona State University with Prof. Matthew D. Green. She received her doctorate in Chemical Engineering at Arizona State University in June 2019, and her research works with Prof. Matthew D. Green have been focused on polymer designs and water desalination membrane developments. Prior to her pursuit of a Ph.D., she obtained her B.E. in Polymer Science and Engineering at Beijing University of Chemical Technology in China in 2014.



Dr. Frederick Beyer is a Materials Research Engineer with the Army Research Laboratory (ARL), located at Aberdeen Proving Ground, MD, USA, and he is currently a Visiting Professor at the University of Sheffield in the United Kingdom. Dr. Beyer's overarching research interest is in self-assembly behaviors in soft materials. Dr. Beyer received his Ph.D. from the University of Massachusetts, Amherst, in 1999, for his work on the effect of block copolymer architecture on morphology. He previously studied Materials Science & Engineering at North Carolina State University before specializing in polymer physics. He has also been active in the polymer physics and chemistry communities, including organizing focus symposia at the 2010 and 2011 American Physical Society March meetings, co-chairing the 2009 American Chemical Society Polymer Chemistry Division workshop on "Advances in Materials and Processes for Polymeric Membrane Mediated Water Purification", and organizing an ACS PMSE Division symposium on "Hierarchically Ordered Functional Materials" in 2007. He was active with the Nanotechnology for Defense Applications Conference, which was designed to bring together researchers and program managers from academia, government laboratories, and industry to facilitate the development of new solutions to Defenserelated technological challenges, serving as Army Chair from 2011 through 2014. In 2012, he was recognized by ARL with the Award for Best Publication and in 2013, he received a Research and Development Award for Outstanding Technical Achievement from the Department

of the Army. He has two patents on applications of reversible chemistry in polymers and has 80 peer-reviewed publications.



Brian Morgan received his undergraduate degree in Chemistry from the College of the Holy Cross in Worcester, MA, and received his doctorate in Polymer Science from the University of Tennessee, Knoxville. He currently works as a postdoctoral researcher at the Army Research Laboratories in Aberdeen Proving Grounds, MD, specializing in the characterization and processing of multifunctional polymeric materials.



Katelyn Kline received her Bachelor's Degree in Chemical Engineering from Arizona State University in 2017. She continued her education at Arizona State University and earned a Master's Degree in Materials Science and Engineering in 2018. Throughout her collegiate experience, she was involved in on-campus research, studying matrix-mixed membranes for water purification, coordination polymers, and polymeric nanocomposites. Upon graduating, she accepted a position as a process engineer with W. L. Gore & Associates, Inc. in Elkton, MD.



Tyler Piper is currently a Production Engineer for Olin Corporation and manufactures liquid epoxy resins in Freeport, TX. He received his Master's Degree in Chemical Engineering at Arizona State University in June of 2018 with his research on material properties of nanoparticle loaded photopolymers, with Prof. Matthew D. Green. Prior to his Master's Degree, he obtained his B.S.E. in Chemical Engineering at Arizona State University in 2017.



Professor Matthew Green joined the faculty at Arizona State University in Chemical Engineering in 2014. His training as a synthetic polymer chemist and chemical engineer positions his research group to sit at the intersection of these disciplines with focused applications in health, the environment, and advanced materials. His laboratory is integrating macromolecular design with controlled synthesis techniques to produce hierarchical and multifunctional materials with particular interest in the interplay between electrostatic interactions and microstructure, interphase interactions, thermomechanical properties, and transport. These features can be used to tune the material properties for applications ranging from membranes for water purification or CO₂ capture to polymeric nanocomposites. Professor Green obtained a B.S. in Chemical Engineering and a B.S. in Chemistry at Virginia Tech in 2007, and a Ph.D. in Chemical Engineering in 2011 at Virginia Tech working with Prof. Timothy Long. Then, he worked as a postdoctoral researcher at the University of Delaware in the Chemical and Biomolecular Engineering Department with Prof. Thomas Epps III and Prof. Millicent Sullivan. He has received several awards, including the Young Membrane Scientist Award (2016) from the North American Membrane Society (NAMS), the NASA Early Career Faculty Award (2018), the Mayo Clinic-ASU Alliance Fellowship (2018), as part of the Mayo Clinic and ASU Alliance for Health Care Summer Residency Program, the Ford Faculty Fellowship (2018), and the NSF CAREER Award (2019).

■ ACKNOWLEDGMENTS

The authors thank the National Science Foundation for financial support, under Grant No. NSF CBET 1836719, and the Army Research Office for support, under Grant No. ARO W911NF-18-1-0412 and DURIP Award No. ARO W911NF-15-1-0353. We acknowledge Prof. L. Dai and Prof. J. Yarger at ASU for providing access to the TGA instruments.

REFERENCES

- (1) Hamid, Z. A. A.; Lim, K. W. Evaluation of UV-crosslinked poly (ethylene glycol) diacrylate/poly (dimethylsiloxane) dimethacrylate hydrogel: properties for tissue engineering application. *Procedia Chem.* **2016**, *19*, 410–418.
- (2) Crosby, A. J.; Lee, J. Y. Polymer nanocomposites: the "nano" effect on mechanical properties. *Polym. Rev.* **2007**, *47* (2), 217–229.

- (3) Ganesan, V.; Jayaraman, A. Theory and simulation studies of effective interactions, phase behavior and morphology in polymer nanocomposites. *Soft Matter* **2014**, *10* (1), 13–38.
- (4) Hall, L. M.; Jayaraman, A.; Schweizer, K. S. Molecular theories of polymer nanocomposites. *Curr. Opin. Solid State Mater. Sci.* **2010**, *14* (2), 38–48.
- (5) Hore, M. J. A.; Composto, R. J. Functional Polymer Nanocomposites Enhanced by Nanorods. *Macromolecules* **2014**, 47 (3), 875–887.
- (6) Kumar, P.; Sandeep, K. P.; Alavi, S.; Truong, V. D. A Review of Experimental and Modeling Techniques to Determine Properties of Biopolymer-Based Nanocomposites. *J. Food Sci.* **2011**, *76* (1), E2–E14.
- (7) Moniruzzaman, M.; Winey, K. I. Polymer Nanocomposites Containing Carbon Nanotubes. *Macromolecules* **2006**, 39 (16), 5194–5205
- (8) Kumar, S. K.; Benicewicz, B. C.; Vaia, R. A.; Winey, K. I. 50th anniversary perspective: are polymer nanocomposites practical for applications? *Macromolecules* **2017**, *50* (3), 714–731.
- (9) Englebienne, P.; Van Hoonacker, A. Gold—conductive polymer nanoparticles: A hybrid material with enhanced photonic reactivity to environmental stimuli. *J. Colloid Interface Sci.* **2005**, 292 (2), 445–454.
- (10) Oh, Y.; Chun, K.-Y.; Lee, E.; Kim, Y.-J.; Baik, S. Functionalized nano-silver particles assembled on one-dimensional nanotube scaffolds for ultra-highly conductive silver/polymer composites. *J. Mater. Chem.* **2010**, *20* (18), 3579–3582.
- (11) Turhan, Y.; Dogan, M.; Alkan, M. Poly (vinyl chloride)/kaolinite nanocomposites: characterization and thermal and optical properties. *Ind. Eng. Chem. Res.* **2010**, *49* (4), 1503–1513.
- (12) Huang, X.-J.; Zeng, X.-F.; Wang, J.-X.; Chen, J.-F. Transparent dispersions of monodispersed ZnO nanoparticles with ultrahigh content and stability for polymer nanocomposite film with excellent optical properties. *Ind. Eng. Chem. Res.* **2018**, *57* (12), 4253–4260.
- (13) Amancio-Filho, S. T.; dos Santos, J. F. Joining of Polymers and Polymer-Metal Hybrid Structures: Recent Developments and Trends. *Polym. Eng. Sci.* **2009**, 49 (8), 1461–1476.
- (14) Giannelis, E. P. Polymer layered silicate nanocomposites. *Adv. Mater.* **1996**, 8 (1), 29–35.
- (15) Paul, D. R.; Robeson, L. M. Polymer nanotechnology: nanocomposites. *Polymer* **2008**, 49 (15), 3187–3204.
- (16) Zhang, H.; Wang, L.; Song, L.; Niu, G.; Cao, H.; Wang, G.; Yang, H.; Zhu, S. Controllable properties and microstructure of hydrogels based on crosslinked poly (ethylene glycol) diacrylates with different molecular weights. J. Appl. Polym. Sci. 2011, 121 (1), 531–540.
- (17) Browning, M. B.; Cereceres, S. N.; Luong, P. T.; Cosgriff-Hernandez, E. M. Determination of the in vivo degradation mechanism of PEGDA hydrogels. *J. Biomed. Mater. Res., Part A* **2014**, *102* (12), 4244–4251.
- (18) Kasaliwal, G. R.; Göldel, A.; Pötschke, P.; Heinrich, G. Influences of polymer matrix melt viscosity and molecular weight on MWCNT agglomerate dispersion. *Polymer* **2011**, 52 (4), 1027–1036.
- (19) Bertrand, O.; Gohy, J.-F. Photo-responsive polymers: synthesis and applications. *Polym. Chem.* **2017**, *8* (1), 52–73.
- (20) Bencherif, S. A.; Srinivasan, A.; Sheehan, J. A.; Walker, L. M.; Gayathri, C.; Gil, R.; Hollinger, J. O.; Matyjaszewski, K.; Washburn, N. R. End-group effects on the properties of PEG-co-PGA hydrogels. *Acta Biomater.* **2009**, *5* (6), 1872–1883.
- (21) Nguyen, Q. T.; Hwang, Y.; Chen, A. C.; Varghese, S.; Sah, R. L. Cartilage-like mechanical properties of poly (ethylene glycol)-diacrylate hydrogels. *Biomaterials* **2012**, *33* (28), 6682–6690.
- (22) Ficek, B. A.; Thiesen, A. M.; Scranton, A. B. Cationic photopolymerizations of thick polymer systems: Active center lifetime and mobility. *Eur. Polym. J.* **2008**, *44* (1), 98–105.
- (23) Anseth, K. S.; Kline, L. M.; Walker, T. A.; Anderson, K. J.; Bowman, C. N. Reaction kinetics and volume relaxation during polymerizations of multiethylene glycol dimethacrylates. *Macromolecules* **1995**, 28 (7), 2491–2499.
- (24) Estridge, C. E.; Jayaraman, A. Effect of homopolymer matrix on diblock copolymer grafted nanoparticle conformation and potential of

- mean force: A molecular simulation study. J. Polym. Sci., Part B: Polym. Phys. **2015**, 53 (1), 76–88.
- (25) Jayaraman, A.; Schweizer, K. S. Effect of the number and placement of polymer tethers on the structure of concentrated solutions and melts of hybrid nanoparticles. *Langmuir* **2008**, *24* (19), 11119–11130.
- (26) Jayaraman, A.; Schweizer, K. S. Effective interactions and self-assembly of hybrid polymer grafted nanoparticles in a homopolymer matrix. *Macromolecules* **2009**, 42 (21), 8423–8434.
- (27) Martin, T. B.; Jayaraman, A. Identifying the Ideal Characteristics of the Grafted Polymer Chain Length Distribution for Maximizing Dispersion of Polymer Grafted Nanoparticles in a Polymer Matrix. *Macromolecules* **2013**, 46 (22), 9144–9150.
- (28) Nair, N.; Jayaraman, A. Self-Consistent PRISM Theory—Monte Carlo Simulation Studies of Copolymer Grafted Nanoparticles in a Homopolymer Matrix. *Macromolecules* **2010**, 43 (19), 8251–8263.
- (29) Gaharwar, A. K.; Peppas, N. A.; Khademhosseini, A. Nanocomposite hydrogels for biomedical applications. *Biotechnol. Bioeng.* **2014**, *111* (3), 441–453.
- (30) Zhan, Y.; Pan, Y.; Chen, B.; Lu, J.; Zhong, Z.; Niu, X. Strain rate dependent hyperelastic stress-stretch behavior of a silica nanoparticle reinforced poly (ethylene glycol) diacrylate nanocomposite hydrogel. *J. Mech. Behavior Biomed. Mater.* **2017**, *75*, 236–243.
- (31) Wang, M.; Dheressa, E.; Brown, K. A.; Green, M. D. Effect of Crosslinker Length and Architecture on the Thermomechanical Properties of CNT-Loaded Elastomeric Polymer Matrix Composites. *Macromol. Rapid Commun.* **2018**, *39*, 1800091.
- (32) Bae, M.; Gemeinhart, R. A.; Divan, R.; Suthar, K. J.; Mancini, D. C. Fabrication of poly (ethylene glycol) hydrogel structures for pharmaceutical applications using electron beam and optical lithography. J. Vac. Sci. Technol., B: Nanotechnol. Microelectron.: Mater., Process., Meas., Phenom. 2010, 28 (6), C6P24—C6P29.
- (33) Janusziewicz, R.; Tumbleston, J. R.; Quintanilla, A. L.; Mecham, S. J.; DeSimone, J. M. Layerless fabrication with continuous liquid interface production. *Proc. Natl. Acad. Sci. U. S. A.* **2016**, *113* (42), 11703–11708.
- (34) Johnson, A. R.; Caudill, C. L.; Tumbleston, J. R.; Bloomquist, C. J.; Moga, K. A.; Ermoshkin, A.; Shirvanyants, D.; Mecham, S. J.; Luft, J. C.; DeSimone, J. M. Single-step fabrication of computationally designed microneedles by continuous liquid interface production. *PLoS One* **2016**, *11* (9), e0162518.
- (35) Tumbleston, J. R.; Shirvanyants, D.; Ermoshkin, N.; Janusziewicz, R.; Johnson, A. R.; Kelly, D.; Chen, K.; Pinschmidt, R.; Rolland, J. P.; Ermoshkin, A.; Samulski, E. T.; DeSimone, J. M. Continuous liquid interface production of 3D objects. *Science* **2015**, 347 (6228), 1349–1352.
- (36) Timur, M.; Paşa, A. Synthesis, Characterization, Swelling, and Metal Uptake Studies of Aryl Cross-Linked Chitosan Hydrogels. *ACS Omega* **2018**, 3 (12), 17416–17424.
- (37) Ilavsky, J.; Jemian, P. R. Irena: tool suite for modeling and analysis of small-angle scattering. *J. Appl. Crystallogr.* **2009**, 42 (2), 347–353.
- (38) Ilavsky, J. Nika: software for two-dimensional data reduction. *J. Appl. Crystallogr.* **2012**, 45 (2), 324–328.
- (39) Dai, X.; Chen, X.; Yang, L.; Foster, S.; Coury, A. J.; Jozefiak, T. H. Free radical polymerization of poly (ethylene glycol) diacrylate macromers: Impact of macromer hydrophobicity and initiator chemistry on polymerization efficiency. *Acta Biomater.* **2011**, *7* (5), 1965–1972.
- (40) Zustiak, S. P.; Leach, J. B. Hydrolytically degradable poly-(ethylene glycol) hydrogel scaffolds with tunable degradation and mechanical properties. *Biomacromolecules* **2010**, *11* (5), 1348–1357.
- (41) Green, D. L.; Lin, J. S.; Lam, Y.-F.; Hu, M. Z. C.; Schaefer, D. W.; Harris, M. T. Size, volume fraction, and nucleation of Stober silica nanoparticles. *J. Colloid Interface Sci.* **2003**, 266 (2), 346–358.
- (42) Frau, A. F.; Lane, T. J.; Schlather, A. E.; Park, J. Y.; Advincula, R. C. Modulating electrochemical activity in polyaniline/titanium oxide hybrid nanostructured ultrathin films. *Ind. Eng. Chem. Res.* **2011**, *50* (9), 5532–5542.

- (43) Caldona, E. B.; De Leon, A. C. C.; Thomas, P. G.; Naylor, D. F., III; Pajarito, B. B.; Advincula, R. C. Superhydrophobic rubber-modified polybenzoxazine/SiO₂ nanocomposite coating with anticorrosion, antice, and superoleophilicity properties. *Ind. Eng. Chem. Res.* **2017**, *56* (6), 1485-1497.
- (44) Cho, J. D.; Ju, H. T.; Hong, J. W. Photocuring kinetics of UV-initiated free-radical photopolymerizations with and without silica nanoparticles. *J. Polym. Sci., Part A: Polym. Chem.* **2005**, 43 (3), 658–670.
- (45) Kane, M. C.; Londono, J. D.; Beyer, F. L.; Brennan, A. B. Characterization of the hierarchical structures of a dry nanopowder in a polymer matrix by X-ray scattering techniques. *J. Appl. Crystallogr.* **2009**, 42 (5), 925–931.
- (46) Jouault, N.; Zhao, D.; Kumar, S. K. Role of casting solvent on nanoparticle dispersion in polymer nanocomposites. *Macromolecules* **2014**, 47 (15), 5246–5255.
- (47) Bera, O.; Pilić, B.; Pavličević, J.; Jovičić, M.; Holló, B.; Szécsényi, K. M.; Špirkova, M. Preparation and thermal properties of polystyrene/silica nanocomposites. *Thermochim. Acta* **2011**, *515* (1–2), 1–5.
- (48) Zou, H.; Wu, S.; Shen, J. Polymer/silica nanocomposites: preparation, characterization, properties, and applications. *Chem. Rev.* **2008**, *108* (9), 3893–3957.
- (49) Chiang, C.-L.; Ma, C.-C. M. Synthesis, characterization, thermal properties and flame retardance of novel phenolic resin/silica nanocomposites. *Polym. Degrad. Stab.* **2004**, 83 (2), 207–214.
- (50) Zhang, F.-A.; Lee, D.-K.; Pinnavaia, T. J. PMMA/mesoporous silica nanocomposites: effect of framework structure and pore size on thermomechanical properties. *Polym. Chem.* **2010**, *1* (1), 107–113.
- (51) Verbeek, C. J. R. The influence of interfacial adhesion, particle size and size distribution on the predicted mechanical properties of particulate thermoplastic composites. *Mater. Lett.* **2003**, *57* (13–14), 1919–1924.
- (52) Fu, S.-Y.; Feng, X.-Q.; Lauke, B.; Mai, Y.-W. Effects of particle size, particle/matrix interface adhesion and particle loading on mechanical properties of particulate—polymer composites. *Composites, Part B* **2008**, *39* (6), 933–961.
- (53) Jankong, S.; Srikulkit, K. Preparation of polypropylene/hydrophobic silica nanocomposites. *J. Met. Mater. Miner.* **2008**, *18* (2), 143–146.
- (54) Hollister, S. J. Porous scaffold design for tissue engineering. *Nat. Mater.* **2005**, *4* (7), 518–524.
- (55) Hayashi, K. Mechanical properties of soft tissues and arterial walls. In *Biomechanics of Soft Tissue in Cardiovascular Systems*; Springer: New York, 2003; pp 15–64.
- (56) Scott, T. F.; Cook, W. D.; Forsythe, J. S. Photo-DSC cure kinetics of vinyl ester resins II: influence of diluent concentration. *Polymer* **2003**, 44 (3), 671–680.
- (57) Abadie, M. J. M.; Xiong, Y.; Boey, F. Y. C. UV photo curing of N,N'-bismaleimido-4, 4'-diphenylmethane. *Eur. Polym. J.* **2003**, 39 (6), 1243-1247.
- (58) Seppala, J. E.; Migler, K. D. Infrared thermography of welding zones produced by polymer extrusion additive manufacturing. *Additive Manufacturing* **2016**, *12*, 71–76.
- (59) Seppala, J. E.; Hoon Han, S.; Hillgartner, K. E.; Davis, C. S.; Migler, K. B. Weld formation during material extrusion additive manufacturing. *Soft Matter* **2017**, *13* (38), 6761–6769.
- (60) Liu, V. A.; Bhatia, S. N. Three-Dimensional Photopatterning of Hydrogels Containing Living Cells. *Biomed. Microdevices* **2002**, *4* (4), 257–266.
- (61) Adzima, B. J.; Tao, Y.; Kloxin, C. J.; DeForest, C. A.; Anseth, K. S.; Bowman, C. N. Spatial and temporal control of the alkyne—azide cycloaddition by photoinitiated Cu(II) reduction. *Nat. Chem.* **2011**, *3*, 256
- (62) Kalsoom, U.; Nesterenko, P. N.; Paull, B. Recent developments in 3D printable composite materials. *RSC Adv.* **2016**, *6* (65), 60355–60371.
- (63) Bowman, C. N.; Kloxin, C. J. Toward an enhanced understanding and implementation of photopolymerization reactions. *AIChE J.* **2008**, 54 (11), 2775–2795.